# From U sequence to Farey sequence: A unification of one-parameter scenarios

John Ringland,* Naoum Issa, and Mark Schell
*Department of Chemistry, Southern Methodist University, Dallas, Texas 75275*
(Received 21 August 1989)

A mechanism is presented and analyzed that accomplishes the unification of a number of experimentally observed one-parameter sequences of dynamical behavior as parts of a continuous spectrum that ranges from the U sequence to Farey sequences. Farey sequences, by which we mean one-parameter sequences whose periodic windows correspond to Farey series of rational numbers, have generally been associated with motion on a state-space torus. The mechanism analyzed here does not involve a torus.

## I. INTRODUCTION

Analyzed in this paper is the transmutation of U sequences into Farey sequences. We are motivated by the existence of a collection of experimentally observed one-parameter sequences, qualitatively distinct and until now without established relationships, that can actually be arranged on a continuous spectrum of behavior. This spectrum runs from the well-known and widely observed U sequence[1,2] through intermediate types of sequence which have also been observed,[3–7] including re-merging period-doubling cascades,[3–5] to sequences resembling phase-locking scenarios on a torus.[8–10] We call the last type Farey sequences because of the correspondence between the set of periodic windows and Farey series[11] of rational numbers. The model presented here, a family of continuous two-extremum maps of the interval, generates the entire spectrum of behavior. The Farey sequences in this model have nothing to do with phase lockings on a torus.

Our analysis takes the following form. In Sec. II we introduce a family of two-extremum maps, which incorporates a parameter by which the steepness between the extrema can be adjusted and made arbitrarily large. We relate this map to examples obtained from experimental data. The full spectrum of one-parameter sequences referred to above is illustrated with orbit diagrams corresponding to a number of values of the steepness parameter. (A U sequence is obtained at low values, a Farey sequence at high values.) In each case, we cite similar observations in experiments and/or differential equations. We then present two-parameter "phase-diagrams" which show how these changing sequences arise as cuts through parameter-plane structures that are *qualitatively unchanged* by the variation of the steepness parameter. These diagrams show that it is rather the *quantitative* evolution of the geometries and positions of these structures that is responsible for the differences among the sequences. In Secs. III and IV we examine the parameter-plane structures in detail, and explain their character, arrangement, and evolution. Section III is devoted to those aspects which are essentially independent of the steepness parameter: the qualitative form of the structures and their qualitative arrangement; and Sec. IV addresses the things which do change as the steepness parameter is varied.

That a mechanism such as the one described here is responsible for some experimentally observed or observable Farey sequences is strongly suggested by the continuous representation of the spectrum of behavior in experimental observations. In Sec. V, in order to guide the attribution of mechanism when a Farey sequence is observed experimentally, we contrast the Farey sequences of two-extremum maps of the interval with those associated with motion on tori.

## II. MAP $Z$ AND ITS PHENOMENOLOGY

### A. Map $Z$

The family of maps we use to illustrate evolution from U sequence to Farey sequence is the following:

$$x_{n+1}=Z(x_n)\ , \tag{1a}$$

where

$$Z(x)\equiv(c+ax)R_s^-(x)+(d+bx)R_s^+(x) \tag{1b}$$

and

$$R_s^{\pm}(x)\equiv\tfrac{1}{2}\pm\tfrac{1}{2}\tanh(sx)\ . \tag{1c}$$

$R_s^{\pm}(x)$ are smoothed step functions between 0 and 1, which "turn off and on" the affine functions they multiply as $x$ changes sign. Thus the map $Z$ approximates a straight line with slope $a$ for $sx$ large and negative, and a straight line with slope $b$ for $sx$ large and positive, and switches between the two in the vicinity of $x=0$. As $s$ becomes progressively larger, the switching is effectively confined to a smaller and smaller interval of $x$. Figure 1 shows the graph of $Z$ for $s=2$, 5, 10, 20, 50, and 1000, at fixed $a$, $b$, $c$, and $d$.

At low $s$ the map $Z$ exhibits the gentle undulation of the two-extremum prototypes, the cubic[12–14] and supercritical sine[15–18] maps. On raising $s$ towards infinity, $Z$ approaches a piecewise-linear limit that has been studied previously.[19,20]

 

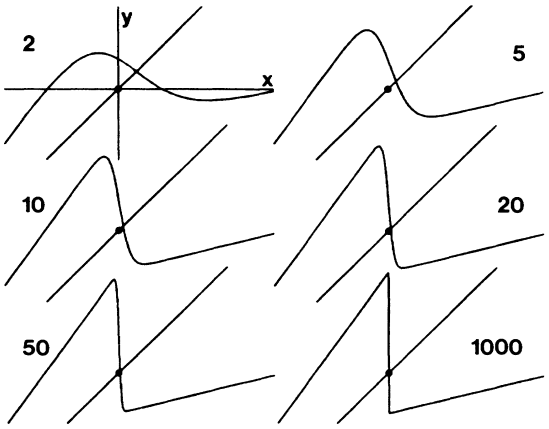


FIG. 1. Graphs of $y=Z(x)$ for various values of the parameter $s$. $a=1.4$, $b=0.25$, $c=1$, $d=-0.4$. The line $y=x$ is included in (a). The scales are the same in all elements, and the ranges are $-1.1<x<1.5$. At low $s$, $Z$ resembles a gently varying cubic polynomial map; at high $s$ it can mimic a monotone map of the circle.

To connect the map $Z$ with experimental systems and differential equations, we refer the reader to several examples of derived maps in the literature. Systems exhibiting gently varying two-extremum maps, represented in $Z$ at low $s$, are commonly observed[21–26] arising generically in the vicinity of homoclinic orbits of saddle-focus type as described in Refs. 23 and 24.

Systems showing more strongly varying maps, like the examples of $Z$ at high $s$ in Fig. 1, are also reported. An example in a truncated mode expansion of the generalized Ginzburg-Landau equation (which models, for example, instabilities in shear fluid flow) is derived in Ref. 27. In observations by Coffman *et al.*[28] of an oscillating chemical reaction, one-dimensional maps constructed from the data have two extrema (marginally, corresponding to low $b$ in $Z$) and a region of very steep slope in the middle, just as our map $Z$ has for large $s$. Decroly and Goldbeter[29] display a map with similar qualities that is exhibited by a set of ordinary differential equations used to model enzyme kinetics; their map also exhibits an angularity which is characteristic of $Z$ at very large $s$. Return maps with angularities and close-to-linear sections have been seen in a number of electrical oscillators.[30]

### B. Orbit diagrams

In Fig. 2 we present a set of orbit diagrams for the map $Z$ which exhibit the spectrum of one-parameter sequences referred to in the Introduction. In each case we cite observations of similar sequences in experiments and/or differential equations.

We begin with the behavior seen in Fig. 2(a) which shows a sequence occurring at $s=5$. This closely resembles sequences seen in numerous experimental observations of forced oscillators.[30–32] Reference 32, for example, shows such a sequence in forced coupled $p$-$n$ junctions, with prominent states of periods 2–7 observed in turn with increasing drive voltage. These are, in fact, U sequences (except possibly at very fine scale). They differ from the prototypical U sequence—that of the logistic map[33]—in the prominence of the windows of the low-period states, which are the states denoted as $RL^m$ ($m=0,1,2,\ldots$) by Metropolis, Stein, and Stein.[34] We digress briefly to describe the different notation employed in the present paper.

Any periodic orbit consists of an alternating series of visits to the left and right sides of the fixed point of $Z$ on the interval where $Z$ has negative slope (see Fig. 1). This fixed point is represented by the curves in Fig. 2 (which are dashed to indicate that the fixed point is unstable). Each right-side visit consists of a sequence of monotonically decreasing iterates, and each left-side visit a sequence of monotonically increasing iterates. As our label for the orbits we simply use the list of the lengths of these visits, superscripting the left-side counts for clarity. Thus the orbit shown in the inset of Fig. 4, for example, is labeled $1^1 1^2$. These labels do not always specify a unique orbit (by unique orbit we mean a unique family of orbits whose iterates have a specific point order on the $x$ axis). Nevertheless, the scheme is convenient and useful, and the distinctions disregarded can be recovered when necessary. Furthermore, it enables direct comparison to be made with results in the literature where analogous schemes are used.[8,9,35–37]

Returning to Fig. 2(a), we note that the principal periodic states, labeled $1^1$, $1^2$, $1^3$, etc., are entered (on decreasing $d$) by tangent bifurcation and excited by period doubling. The region between adjacent principal-state windows is occupied by the period-doubling cascade of the lower-period principal state, and by chaotic and long-period states.

Figure 2(b) shows the second kind of one-parameter sequence, occurring on the path at $s=7.5$ that is otherwise the same as that of Fig. 2(a). This sequence is quite similar to that of Fig. 2(a), except that the principal-state windows are interrupted by "period-bubbling"[3–5] phenomena, i.e., incomplete, re-merging, period-doubling cascades. Such sequences have been observed in models of magnetoconvection[3] and of acoustically induced fluid cavitation,[5] and other driven systems including Duffing's oscillator.[4]

The third kind of behavior is represented by the sequence shown in Fig. 2(c) where $s=10$. [The path is otherwise the same as in Figs. 2(a) and 2(b)]. The principal windows are now entered not by tangent bifurcation, but by period halving. Sequences with these characteristics have also been seen in experiments[6] and differential equations.[7]

The remaining two parts of Fig. 2 show the establishment of the Farey sequence. The sequence of Fig. 2(d) ($s=20$) is similar to that of (c) but for the notable presence of new periodic windows between the principal windows. The periods are the sum of the periods of adjacent principal states, and the labels, e.g., $1^1 1^2$, are the concatenation of the labels of the adjacent principal windows. These periodic states are the Farey mediants[9] of the principal states. Also to be seen in (d) is a period-3 state ($2^1$) to the right of the period-2 state ($1^1$). This is a

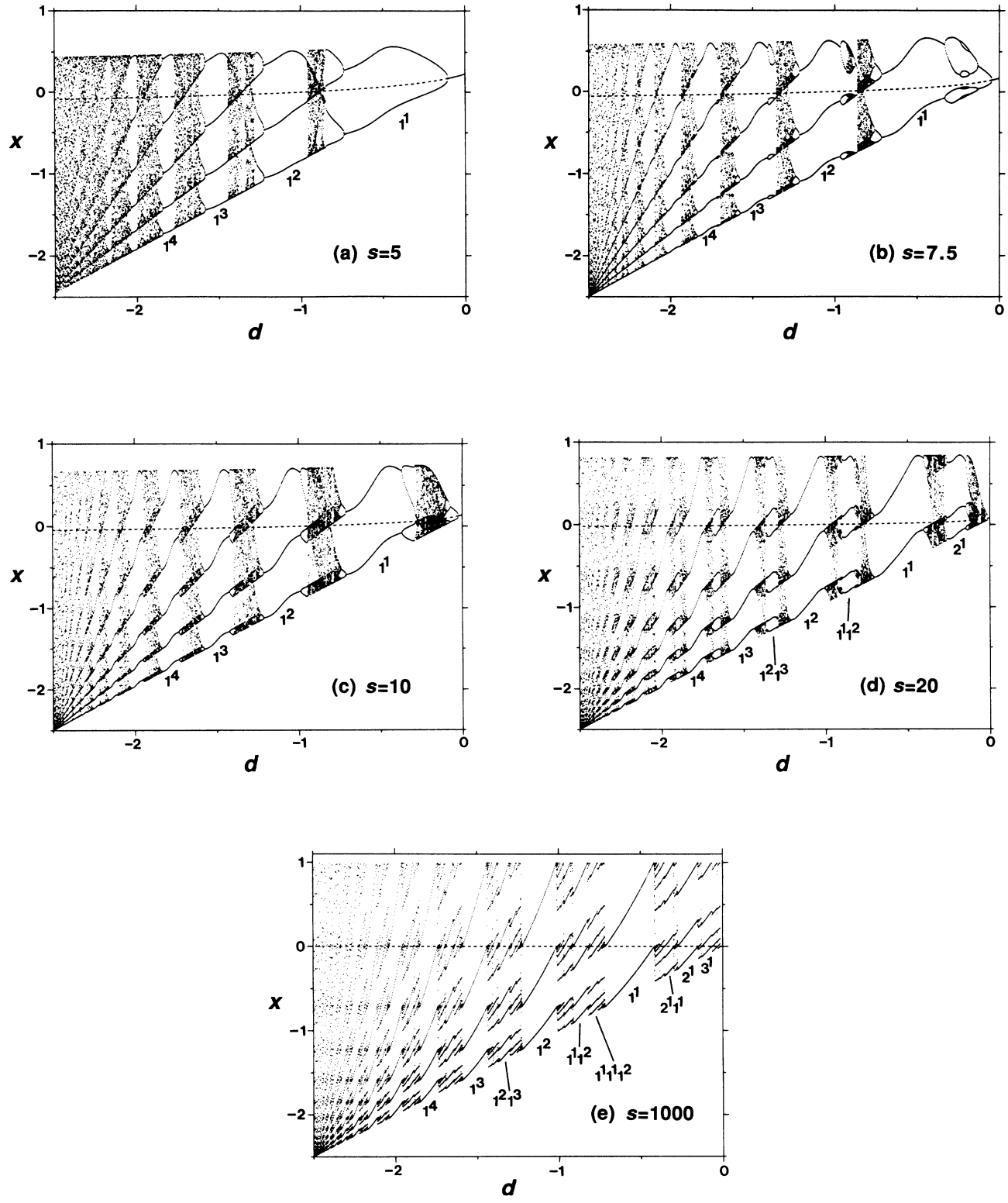


FIG. 2. Orbit diagrams for the map $Z$ with $a=1.4$, $c=1$, $b=\frac{1}{2}(1+d/2.5)$, at five different values of $s$. The labeling of states is explained in the text. The dashed curve represents the unstable period-1 orbit. (a) $s=5$. A U sequence. The principal periodic windows are entered (right to left) by tangent bifurcation and exited by period doubling. (b) $s=7.5$. A sequence similar to that in (a) but exhibiting the period-bubbling phenomenon. (c) $s=10$. A sequence in which the principal periodic windows have period-doubling boundaries on both sides. (d) $s=20$. Similar to (c) but with the appearance of Farey intermediate states. (e) $s=1000$. Two well-developed Farey sequences, one going each way from the $1^1$ window.

member of a second sequence going the other way (with principal states $1^1, 2^1, 3^1, \ldots$) that is more fully realized in Fig. 2(e). Experimental examples of sequences like that of Fig. 2(d) are reported in Ref. 37.

Figure 2(e) is the diagram for $s = 1000$, and shows a pair of Farey sequences that are well developed in the sense that a set of periodic windows exists which correspond to a Farey series of high order;[11] between the $1^1$ and $1^2$ windows is a $1^1 1^2$ window, between the latter two is a $1^1 1^2 1^2$ window, and so on to a substantial depth. The windows corresponding to Farey series account for a large fraction of the total measure of the sequence; period-doublings and chaos occur in very small gaps between them.

We note the superficial similarity of Figs. 2(d) and 2(e) with Fig. 4 of Ref. 10, which depicts Farey sequences whose mechanism is phase locking between intrinsic and external oscillators in a model of a driven nonlinear optical system. Less certain are the mechanisms behind experimental observations of similar sequences.[8,9] Means

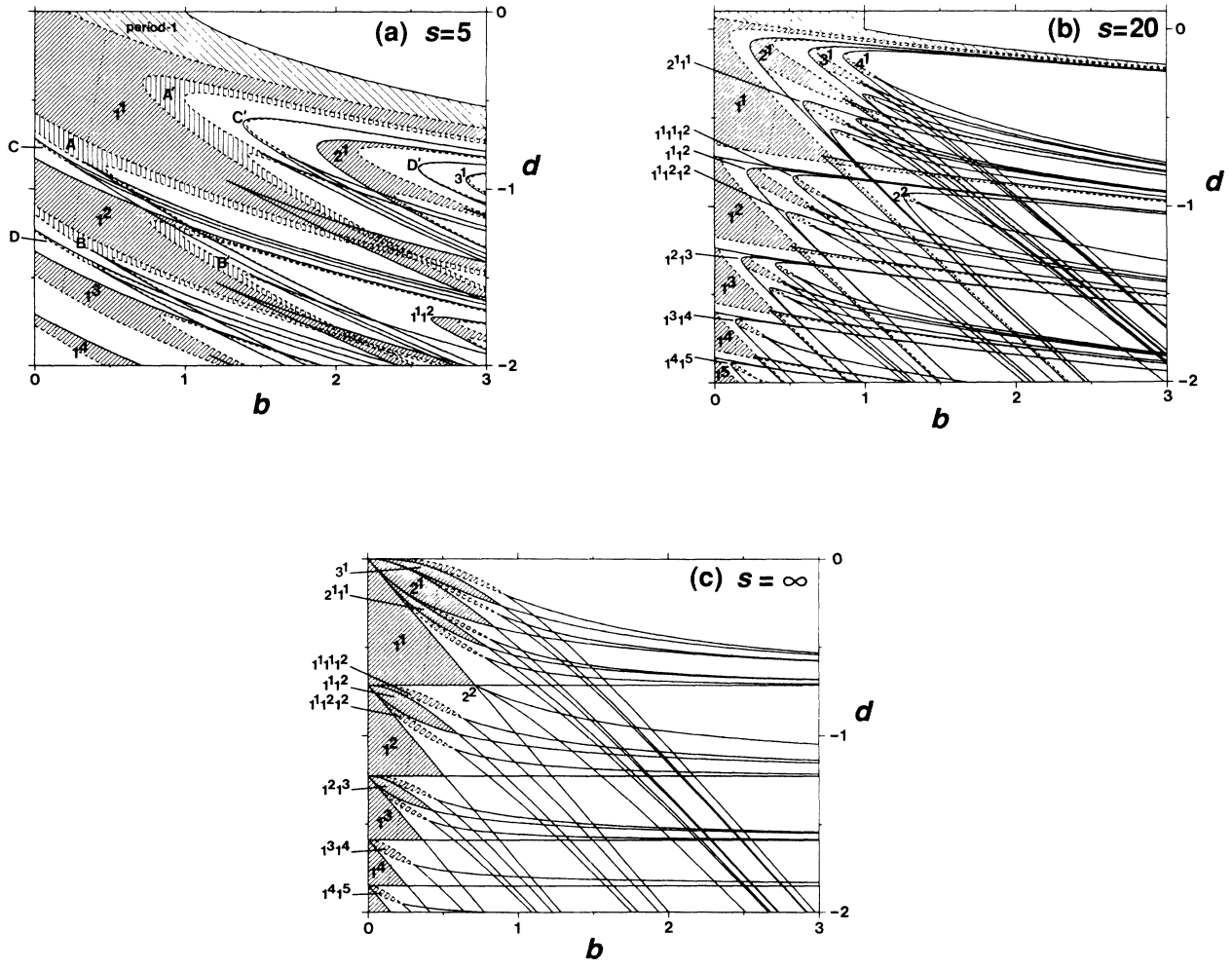


FIG. 3. Phase diagrams for the map $Z$. Computed cross sections of the parameter space at $a = 1.4$, $c = 1.0$. (a) $s = 5$, (b) $s = 20$, (c) infinite $s$. Hatched regions show where periodic states of interest are stable. Solid and dashed curves denote tangent and period-doubling bifurcation curves, respectively. The dotted lines show the paths of the orbit diagrams of Fig. 2. The "negative-slope" diagonal hatching indicates stability of the central fixed point. Positive-slope hatching is used for periodic states with no essential iterate on the interval between the map's turning points. The labeling of these regions is explained in the text. Other periodic regions shown (vertical hatching) in (a) the doublings of the $1^1$ state, $A$ and $A'$, the doublings of the $1^2$ state, $B$ and $B'$, and the period-5 U-sequence states labeled $C$, $C'$, $D$, and $D'$. $C$ and $C'$ are $RLR^2$ (see Ref. 34) with respect to the maximum and minimum, respectively; $D$ and $D'$ are similarly $RL^2R$. These regions become too thin to show in (b) and (c). The change in character of the one-parameter sequences of Fig. 2 as $s$ is increased is associated with changes in the geometry, not the topology, of the orbits' stability regions, and with the migration of the stability regions corresponding to Farey-sequence orbits, such as $1^1 1^2$, from high to low $b$.

by which the mechanisms may be established for behavior of this kind to be observed in future experiments is discussed in Sec. V.

### C. Phase diagrams

To obtain a broader perspective on the sequences of Fig. 2, we show in Fig. 3 two-parameter phase diagrams corresponding to three of the $s$ values sampled in Fig. 2. The paths of Fig. 2 are shown as dotted lines. These phase diagrams display the regions of the $(b,d)$ parameter plane (hatched) where periodic orbits of interest exist and are stable. We refer to each of the stability regions as the "body" of the corresponding orbit.

The body of the $1^1 1^2$ orbit is selected for detailed description and labeling in Fig. 4. The curves that define the body are loci of tangent and period-doubling bifurcation. They are computed by solving the following equations (for a period-$p$ orbit):

$$Z^p(x)=x\ ,$$

$$\frac{dZ^p}{dx}(x)=\begin{cases}+1 \text{ for tangent bifurcation}\\ -1 \text{ for period-doubling bifurcation}\end{cases} \tag{2}$$

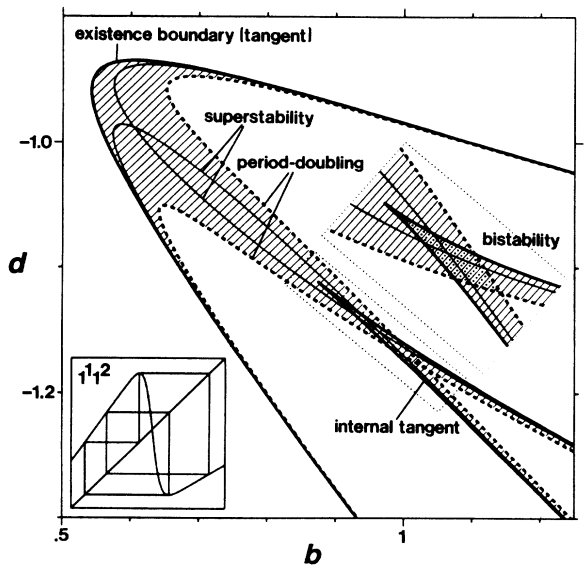


FIG. 4. The region of stability, or body, of a periodic orbit ($1^1 1^2$ at $a=1.4$, $c=1$, $s=10$). Iteration of the map at a representative point within this region is shown in the lower inset. In the main figure and the enlargement, thick solid and dashed curves denote tangent and period-doubling bifurcation loci, respectively. Along the thinner solid curves a superstable (eigenvalue zero) orbit exists. The hatching indicates the region where a stable orbit exists. The internal tangent bifurcation curve corresponds to the folds of a pleat in the surface in (state)×(parameter) space on which the orbit exists; in the diamond-shaped region that is stippled in the enlargement two orbits are simultaneously stable. Orbits that arise as the doublings of others have a period-doubling bifurcation as their existence boundary, rather than a tangent bifurcation, but their bodies are otherwise qualitatively the same.

using standard numerical continuation techniques. In the case shown, the existence boundary is a locus of tangent bifurcation; for orbits which arise as the doubling of another, the existence boundary is a period-doubling bifurcation locus (of the other). This is the only respect in which bodies of the periodic orbits differ qualitatively one from another. Everywhere on one side of the existence boundary (the lower right in the figure) there exists at least one orbit of the period and point order under consideration. The two curves meeting in a cusp form the "internal" tangent bifurcation locus; they constitute the folds of a pleat in the surface in (parameter)×(state) space on which the orbit exists. The two dashed curves are period-doubling bifurcation loci. The hatching shows where at least one stable orbit exists. In the diamond-shaped region that is stippled in the enlargement, two versions of the orbit are simultaneously stable. We will refer to the narrow parts of the hatched region as the "arms" and "legs" of the orbit's body, and to the rest as its "torso."

Also shown within the body in Fig. 4 are loci of singly superstable orbits (SSO's) with eigenvalue zero. These are the two curves on which a periodic orbit exists that includes one of the turning points of the map; one curve is associated with the left turning point, the other with the right turning point.[38] At one of the points where the two curves cross (the one on the right in Fig. 4), which we call the bi-SSO, two singly superstable versions of the orbit coexist. The other intersection of the two curves is the location of a doubly superstable orbit (DSO): a periodic orbit that includes both turning points of the map. The representative orbit shown in the lower inset is, in fact, doubly superstable.

Figure 3(a) contains the path of Fig. 2(a), shown by the dotted line. The prominent bodies marked $1^1$, $1^2$, $1^3$, etc. through which this path cuts correspond to the principal periodic windows of the sequence of Fig. 2(a). These bodies, which have one arm in the unshown negative-$b$ region, have tangent bifurcations as their exterior boundary. Thus a path that intercepts these principal orbits' bodies in the manner of Fig. 2(a) enters each (top to bottom) through a tangent boundary, and leaves through a period-doubling boundary. As mentioned earlier, these bodies correspond to the orbits denoted as $RL^m$, $m=0,1,2,\ldots$, by Metropolis, Stein, and Stein.[34] Bodies of other U-sequence orbits are also shown: doubled $1^1$ ($RLR$) orbits, and the period-5 orbits $RLR^2$ and $RL^2R$ (two of each, one associated with each extremum).

Figure 3(b) contains the path of Fig. 2(c). The diagram is qualitatively similar to Fig. 3(a), but the elevation of $s$ to 20 has greatly narrowed the arms of the principal bodies (the gap between the exterior tangent and period-doubling curves), and pulled the lower parts of where the arms and torsos merge much closer to $b=0$. It is the transit of these merging parts across the one-parameter path, between $s=5$ and 7.5, that is responsible for the period bubbling in Fig. 2(b). The periodic state appears by tangent bifurcation as the arm is entered, doubling occurs as the arm is exited, and the state restabilizes by period halving as the torso is entered. Destabilization again occurs by doubling, as in Fig. 3(a), where the path

passes out through the other side of the torso.

Once $s$ is as large as 10, the arm of stability is, in fact, so thin that it is unresolvable in the orbit diagram of Fig. 2(c); the state is not readily observable until is restabilizes by period halving as the torso of the body is entered. In this way what is for practical purposes a halving-in–doubling-out sequence is obtained, though the true entrance boundary of the principal windows is still a tangent bifurcation located at some distance from the observable halving boundary.

Figure 3(b) shows bodies of orbits which are not present in Fig. 3(a). These correspond to the intermediate states of the principal states in the Farey sequence. The increase in $s$ has caused these bodies to migrate in from higher $b$ values. The body of the mediant $1^1 1^2$ of the $1^1$ and $1^2$ principal states is actually visible in the lower right-hand corner of Fig. 3(a). At $s=20$, the bodies of only the direct mediants of the principal orbits have crossed the one-parameter path, as in Fig. 2(d), but as $s$ becomes larger, the bodies of more orbits from deeper in the Farey sequence are squeezed into the regions under the parts of the principal bodies where an arm and torso merge, and the Farey sequence orbits become a progressively more preponderant feature of sequences observed on paths which pass through the torsos of the principal bodies. The orbits that necessarily visit the negative-slope interval, such as $RLR^2$ and $RL^2R$, are simultaneously squeezed out. We note that in the Farey sequences of the map $Z$, such as that shown in Fig. 2(b), the (apparent) boundaries of the principal bodies are period doublings (outwards), as are those of all of the Farey intermediate states except those just marginally established [e.g., the $1^4 1^5$ in Fig. 3(b)].

Figure 3(c), which is the analytically computed diagram for $Z$ in the infinite-$s$ limit, is a good approximation of the picture for $s=1000$, the value for the orbit diagram of Fig. 2(c). A complete Farey sequence exists with full measure on the one-parameter path shown by the dotted line (and on all similar paths).[19,20] For practical reasons only a relatively small number of bodies is shown, of course. Figure 3(c) may be compared with figures in Refs. 19 and 39.

We have now established the continuity of the various experimental behaviors cited in Sec. II A in terms of the qualitative invariance of the two-parameter phase diagram as the steepness parameter is varied. The observed differences are due to relative motions of the bodies of the periodic orbits and to quantitative changes in their geometry.

In Sec. III, the qualitative character of the bodies and of their arrangement in the plane are explained. In Sec. IV, their changing aspects as $s$ tends to infinity are addressed.

## III. UNCHANGING ASPECTS OF THE PHASE DIAGRAMS

### A. Explanation of the qualitative features of a body

All the bodies in Fig. 3 have the same basic form. This result implies that the form has little to do with the specifics of any orbit or the detailed shape of the map. Indeed such bodies have been seen in numerous other systems.[12,13,17,18,25,26,40,41] Yet no explanation has been offered to date for the form of these structures. Below we present a graphical explanation of the qualitative structure of a body. In so doing, we establish the location of a DSO as the organization center of the body. In Sec. III B we present results on the arrangement and movement, with respect to variations in $s$, of the DSO locations—results which will then be understood also to apply to the arrangement and movement of the bodies.

We consider the vicinity of a DSO location and show that the form of the body of an orbit is a simple geometric consequence of the two-extremum character of the map. Figure 5(a) depicts schematically the situation at a point in the parameter plane of a map $f$ slightly displaced from site of a DSO of period $j+k$. Here $j$ iterations of the map starting from the left turning point yield a point displaced by a small amount $\lambda$ from the right turning point, and likewise the $k$th iterate of the right turning point misses the left turning point by some small amount $\mu$. (Any multiple composition of $f$ has a turning point at a turning point of $f$ itself.)

The graph of the identity map (the "45° line") facilitates the visualization of these facts. But to investigate graphically the dynamics near this condition we use a "one-stroke" iteration method rather than the standard "two-stroke" technique that uses the identity map. The need for the graph of the identity map is eliminated by drawing the graph of $f^j$ "sideways." That is, we draw the graphs $\{(x,y)|x=f^j(y)\}$ and $\{(x,y)|y=f^k(x)\}$. Iteration is then achieved by each intergraph stroke. Figure 5(b) depicts the situation of Fig. 5(a) in the one-stroke representation; the displacements $\lambda$ and $\mu$ are visible directly. Figure 5(c) shows, in the same representation, the situation right at the site of the DSO, where the turning points are mapped exactly to one another.

If we consider the displacements $\lambda$ and $\mu$ in Fig. 5 to be the numerical values of two parameters, we make possible a direct graphical construction of the structure that surrounds a DSO location. We carry this out in Fig. 6.

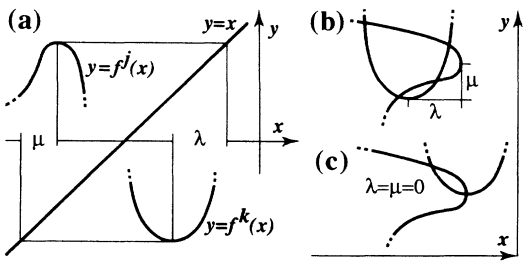


FIG. 5. Schematic iteration of a map $f$ near a DSO of period $j+k$. (a) Standard two-stroke technique using $y=f^j(x)$ near the left turning point, $y=f^k(x)$ near the right turning point, and $y=x$. (b) One-stroke technique. Graphing $x=f^j(y)$ and $y=f^k(x)$ obviates the need for $y=x$. The periodic orbit is represented by an intersection of the two graphs, and bifurcations and superstability correspond to simple geometric configurations. (c) The DSO in the one-stroke representation.

The effect of varying parameters will be primarily to shift the upright and sideways graphs relative to each other. The qualitative aspects of the structure are due to this relative motion, not to any accompanying changes in shape. So in Fig. 6, with negligible loss of generality, the shapes of the graphs are taken to be unaffected by the parameters; only their positions change. We choose the reference frame in the $(x,y)$ plane in which the sideways graph (it is the curve which projects beyond the frame to the left) is fixed. Varying parameters thus affects only the position of the upright graph. The tip $(+)$ of the upright graph, which is taken to have coordinates $(\lambda,\mu)$, then traces out the loci of interest in the effectively superimposed parameter plane $(\lambda,\mu)$ as the upright graph is moved in such a way as to maintain the corresponding geometrical condition. The graphs have been drawn with blunt tips for diagrammatic clarity, as this has the effect of increasing the spacing of the loci of interest.

The loci of three conditions are constructed: (i) superstable orbit, which exists when the graphs intersect at the tip of one of them; (ii) tangent bifurcation (tangency of the graphs); and (iii) period-doubling bifurcation which arises when, at their intersection, the graphs have slopes of the same magnitude and opposite sign (since one graph is sideways, the eigenvalue is given by the quotient of the slopes). For each locus, at least one example of the upright graph's position is shown. The schematic loci obtained in this way are qualitatively identical (except for orientation) to the numerically computed ones for the $1^1 1^2$ orbit of $Z$ shown in Fig. 4.

We have assumed that the orbit (intersection of the graphs) which exists to the upper left of the DSO as in Fig. 5(b) is of the same period as the DSO. It is possible that its period is half that of the DSO. In this case, raising the upright graph will result not in a collision of two fixed points corresponding to a tangent bifurcation, but to a collision of three fixed points corresponding to a period halving.

### B. Qualitative arrangement of the states

Having shown how the qualitative form of the bodies is a property of the geometric interaction of two arcs near where they intersect tip to tip, i.e., the point of existence of a DSO, we now discuss the organization of the DSO's. In the following we will, for convenience, use the term DSO to refer to the parameter-plane location of a doubly superstable orbit, as well as to the orbit itself; which meaning is intended will be clear from context.

The organization in the $(b,d)$ plane of the DSO's of the orbits that can be characterized as $N^m$ using our previously established notation can be understood with the aid of Fig. 7, where 16 such orbits are pictured. First, we note that the portion of the map to the left of $x=0$ is barely affected by the parameters $b$ and $d$, as long as $s$ is not too small (all panels of Fig. 7). Secondly, the larger the asymptotic slope of $Z$ on the right (i.e., $b$), the more

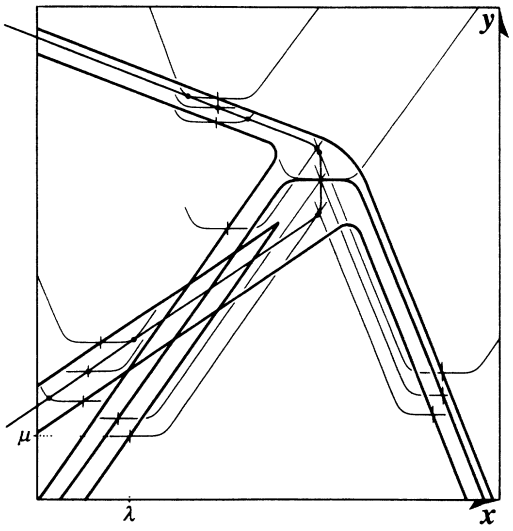


FIG. 6. Geometric explanation of the qualitative character of the body of a periodic orbit. The curve extending beyond the frame to the left represents the sideways arc of Fig. 5. The $(x,y)$ position of the tip $(+)$ of the upright arc is taken to be numerically equal to the values of parameters $\lambda$ and $\mu$. In this way the parameter and state spaces are superimposed and the body appears as the locus of the tip of the upright arc as the appropriate geometric relations between the arcs are maintained: tangency for tangent bifurcation; slopes at intersection of equal magnitude but opposite sign for period-doubling; intersection at a tip for superstability.

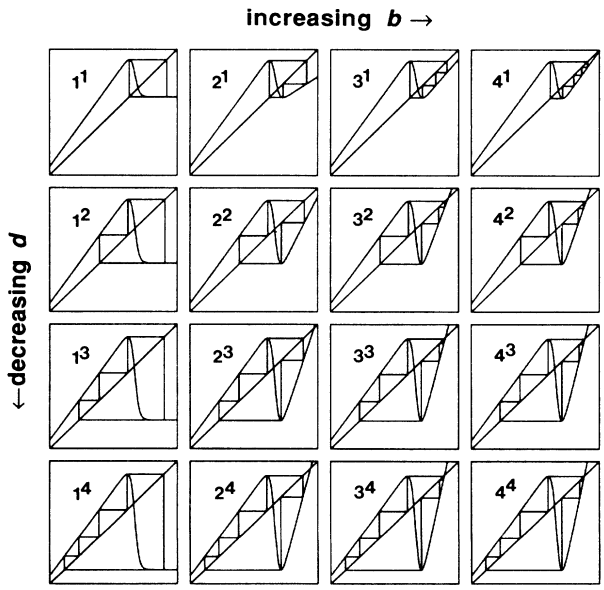


FIG. 7. DSO's of some of the $N^m$ orbits in $Z$. $a=1.4$, $c=1$, $s=10$. Increasing $b$ permits more consecutive iterates on the right side of the central fixed point. Making $d$ more negative permits more consecutive iterates on the left side of the fixed point. This accounts roughly for the $(b,d)$-plane arrangment of the bodies of these orbits.

consecutive iterates on the right are possible (across any row of Fig. 7). Thirdly, the more negative is $d$, the lower is the minimum of $Z$, and therefore the more consecutive iterates are possible on the left (down any column of Fig. 7). Thus, regardless of the value of $s$, we expect an arrangement of the $N^m$ orbits in the $(b,d)$ parameter plane roughly as the elements are arranged in Fig. 7.

More precisely, the DSO's of the $N^m$ orbits lie at the intersections of the curves shown, for $s=10$, in Fig. 8. Each of these curves is the locus of existence of a specific itinerary between one turning point of $Z$ and the other. One set (dotted) corresponds to itineraries from the left turning point to the right one, and the other set (dashed) to itineraries from the right one to the left one. We call these loci of inter-turning-point itineraries "$I$ curves." The intersection of a dotted $I$ curve with a dashed $I$ curve corresponds to a closed orbit that includes both turning points, i.e., a DSO.

The gain from considering the net of $I$ curves is that we can speak of the topology of the net of $I$ curves whose nodes are the DSO points. The topology exhibited in Fig. 8 is a persistent feature of the $(b,d)$ parameter plane; there is complete transversal intersection of the two sets of $I$ curves for $s$ greater than approximately 5, and in this sense the arrangement of the $N^m$ DSO's is qualitatively persistent for $s$ above this value.

While they are fundamental, the $N^m$ orbits are only a small subset of the periodic orbits of the map. The DSO's of the other orbits arise due to families of $I$ curves which emanate from every DSO, as described in detail in Refs. 42 and 43. Here we illustrate in Fig. 9 the dynamics near a DSO with the one-stroke representation in such a way as to explain the character of the emanating $I$ curves and to show how they give rise to other important

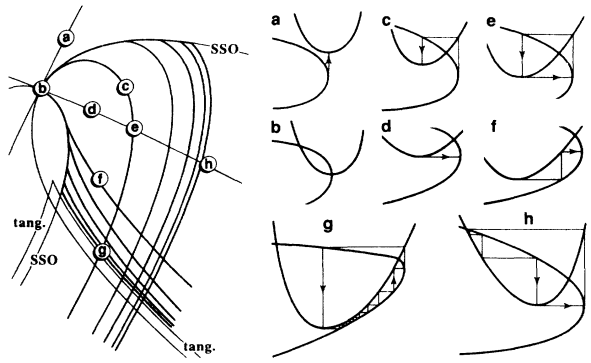


FIG. 9. Sketches illustrating the parameter-plane vicinity of a DSO. The left panel shows the $I$ curves emanating from a DSO. The small pictures on the right show the behavior of the map in the one-stroke representation of Fig. 5 at selected points. A U sequence is generated along $bh$, and the intersections with $eg$ of the emanating curves like $bf$ and $bg$ constitute part of a Farey sequence. See text for a more detailed description.

DSO's. The diagrams on the right of the figure depict in the one-stroke representation the dynamics at the labeled points in the parameter-plane vicinity of a DSO shown on the left. The figure illustrates the role of the $I$ curves emanating from the DSO at $b$ in generating a U sequence of DSO's along the $I$ curve $bdeh$; the DSO at $e$ is the doubling of the one at $b$. The other shown half-bundle of emanating $I$ curves is part of a Farey tree;[43] for example, the DSO at the intersection of $bf$ and $bceg$ is the Farey mediant of those at $b$ and $e$. In Fig. 10 we show numerical results for the map $Z$. As well as showing the $I$ curves that "cause" the $1^1 1^2$ and $1^1 1^1 1^2$ DSO's, we show the $I$ curve (analogous to $bceg$ in the sketch of Fig. 9)

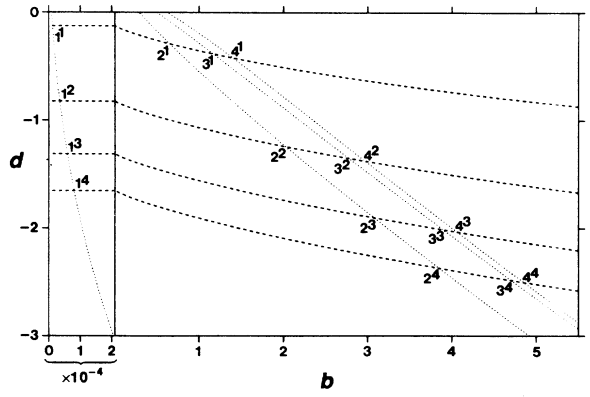


FIG. 8. The doubly superstable orbits $N^m$ of the map $Z$ exist at the intersections of $I$ curves, the loci of inter-turning-point itineraries. Dashed (dotted) curves correspond to itineraries from the left (right) turning point to the right (left) one. The first four members of each family are shown. $a=1.4$, $c=1$, $s=10$. For clarity, there is a scale change at $b=2.1\times10^{-4}$. The complete transversal intersection of these two families of curves is a robust of the $(b,d)$ plane for $s\gtrsim 5$. Iteration of the map at each of the intersections is shown in Fig. 7.

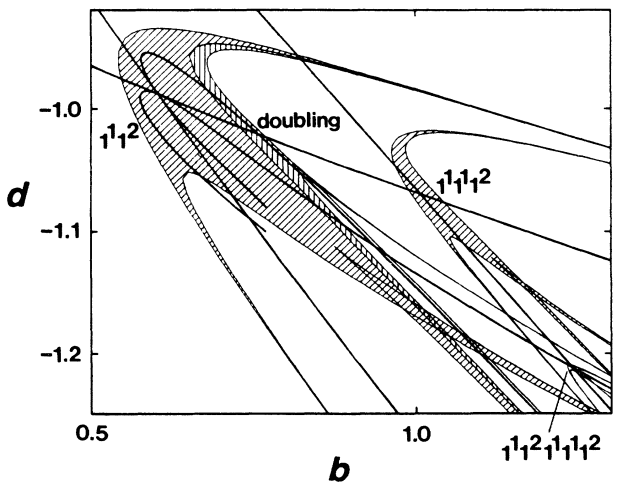


FIG. 10. Numerical calculations showing the emanating $I$ curves which give rise to the doublings of $1^1 1^2$ and the Farey intermediate state $1^1 1^2 1^1 1^1 1^2$ of $1^1 1^2$ and $1^1 1^1 1^2$. $I$ curves are the thicker curves. $a=1.4$, $c=1$, $s=10$.

emanating from the $1^1 1^2$ DSO which causes the DSO of the doubling of the $1^1 1^2$ orbit, and the $I$ curve (analogous to $bf$ in the sketch of Fig. 9) emanating from the $1^1 1^2$ DSO which causes the DSO of the Farey mediant $1^1 1^2 1^1 1^1 1^2$ of the $1^1 1^2$ and $1^1 1^1 1^2$ orbits.

The existence of the emanating $I$ curves and their local arrangement is a robust feature of the general DSO. Their global behavior is also subject to strong constraints, so that the topology of the complete and exceedingly intricate $I$-curve network—and thus, in the same sense as before, of the arrangement of DSO's—is expected to be independent of the parameter $s$ (again for $s$ greater than approximately 5).[44] This invariant arrangement is also yielded by the kneading theory[41,45] under rather general assumptions about the nature of the two-extremum map.

## IV. CHANGING ASPECTS OF THE PHASE DIAGRAMS

### A. Motion of DSO's

We analyze the differences among the elements of Fig. 3 first in terms of the motions of the DSO's toward their limiting positions as $s$ goes to infinity. These motions are illustrated in Fig. 11 where the $(b,d,s)$ paths of selected DSO's are shown for $s$ increasing from the value 5. The $(b,d)$ projections are shown on the top plane of the cubes. Every DSO that has an iterate on the interval between the turning points of the map has the same infinite-$s$ asymptote as one that does not. We therefore consider first the class of DSO's, represented in Fig. 11, which do not (since their asymptotes constitute the complete set of DSO asymptotes).

Consider the fact that $Z(x_R)-Z(x_L)$, if $x_L$ and $x_R$ are

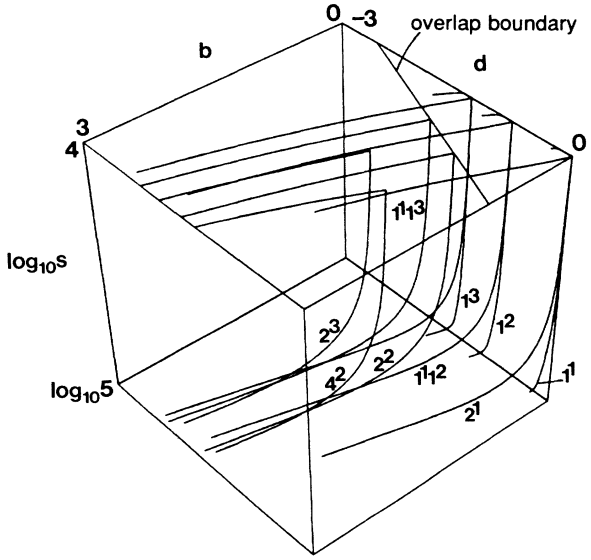


FIG. 11. Paths of selected DSO's in the $(b,d,s)$ parameter space of $Z$ illustrating the approach to the infinite-$s$ asymptotes. The $(b,d)$ projections are shown on the top surface. DSO's not involving overlap are asymptotic to $b=0$; examples are $2^1$, $1^1$, $1^1 1^2$, $1^2$, and $1^3$. DSO's relying on overlap are constrained from lying on the low-$b$ side of the overlap boundary; examples are $2^2$, $1^1 1^3$, $4^2$, and $2^3$.

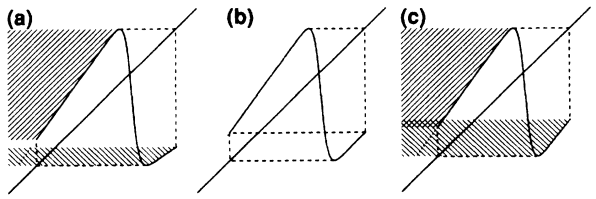


FIG. 12. The map $Z$ (a) ($b=0.7$) "below," (b) ($b=1.02$), on, and (c) ($b=1.3$) "above" the overlap boundary. Below the overlap boundary, $Z$ restricted off the negative-slope interval is one to one. This boundary plays a major role in the organization of DSO's. $a=1.4$, $c=1$, $d=-1.653\,16$, $s=10$.

the left and right turning points of $Z$ respectively, is nonzero (actually $d-c$) in the infinite-$s$ limit, and yet for a DSO of period $p$, $Z^p(x_R)-Z^p(x_L)=x_R-x_L$ vanishes in the limit. This means that if at a DSO we simultaneously follow the itineraries of the two turning points, the finite separation which arises on the first application of the map must be negated in the course of the rest of the iteration. There are only two ways in which this can happen. The itineraries can be brought together either (i) because a forward point has two preimages, or (ii) if the slope $b$ vanishes. But only to the high-$b$ side of a curve we call the *overlap boundary,* defined by

$$Z^2(x_L)=Z^2(x_R)\ , \tag{3}$$

does $Z$, restricted off the interval between the turning points, have points with two preimages: Fig. 12 shows the map on the overlap boundary and on both sides of it. Therefore DSO's relying on preimage duplicity are constrained to lie on the high-$b$ side of the overlap boundary, which in the limit is given by

$$\frac{d}{c}=\frac{1-b}{1-a}\ . \tag{4}$$

Examples of such DSO's in Fig. 11 are $4^2$ and $2^3$ (see Fig. 7) with asymptotes some distance beyond the overlap boundary on the high-$b$ side, and $2^2$ and $1^1 1^3$, which require only marginal overlap and are asymptotic to the overlap boundary itself.

DSO's that do not involve overlap are asymptotic to $b=0$. Those of the principal periodic states and all their Farey intermediate-states fall into this class. The encroachment from high to low $b$ of the bodies of the Farey intermediate orbits, and the resulting appearance of these orbits in the orbit diagram of Fig. 2(c), is due to the motion of their DSO's towards infinite-$s$ asymptotes on $b=0$. Examples of DSO's asymptotic to $b=0$ shown in Fig. 11 are $2^1$, $1^1$, $1^1 1^2$, $1^2$, and $1^3$. Note that at $b=0$ only a discrete set of $d$ values permit an itinerary from the minimum to the maximum. This accounts for the clustering of DSO's at the points,

$$b=0,\quad \frac{d}{c}=-\frac{1-a^{k-1}}{a(1-a)},\quad k=1,2,3,\ldots\ . \tag{5}$$

Now we consider the class of DSO's which do have iterates on the interval between the turning points. Be-

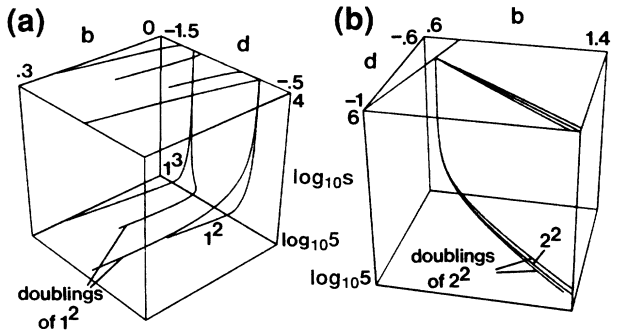


FIG. 13. Motion of other selected DSO's in the $(b,d)$ plane of $Z$ as $s$ tends to infinity, showing the asymptotic degeneracy of DSO's having iterates on the negative slope interval with those that do not. (a) The two doublings of $1^2$ becoming degenerate with $1^2$ and $1^3$. (b) $2^2$ and its two doublings all tending to the same point on the overlap boundary. $s=1.4$, $c=1$.

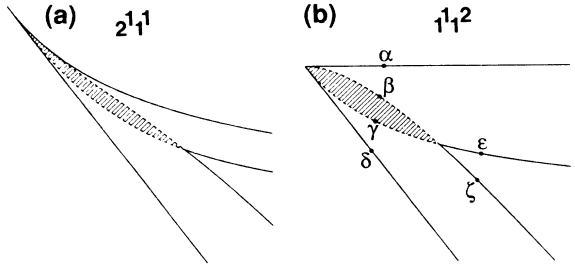


FIG. 14. To clarify Fig. 3(c), the bodies of (a) the $2^1 1^1$ and (b) the $1^1 1^2$ orbits in the infinite-$s$ limit are shown in isolation. $a=1.4$, $c=1$.

cause this interval vanishes in the limit, every DSO with a point on that interval must become degenerate with the DSO of shorter period obtained by truncating the former at its first visit to the interval. The approach to this degeneracy is illustrated for several examples in Figs. 13(a) and 13(b). Figure 13(a) shows the motion of the DSO's of the two doublings of the $1^2$ orbit. One becomes degenerate with the $1^2$ DSO and the other with the $1^3$ DSO. Figure 13(b) shows the DSO of the $2^2$ orbit and those of its two doublings all approaching the same point on the overlap boundary. Note that in the limit the wedge between the overlap boundary and $b=0$ is entirely devoid of DSO's.

The most important result of this subsection is that the encroachment from high to low $b$ of the bodies of the Farey intermediate states is due to their DSO's having infinite-$s$ asymptotes on $b=0$, for reasons explained.

### B. Evolution of the bodies

The motions of the DSO's to their infinite-$s$ asymptotes are accompanied by geometrical changes in the bodies that the DSO's drag along. To emphasize that these geometrical changes are qualitative only, and to resolve any confusion caused in Fig. 3(c) by the concurrence of dashed and solid curves, we reproduce in Figs. 14(a) and 14(b) two bodies from Fig. 3(c) in isolation. The six labeled points of the $1^1 1^2$ body in Fig. 14(b) are illustrated in the one-stroke representation in Fig. 15; in the limit the arcs of the construction become angular. This angularity means that condition $\alpha$ is a degeneracy of tangency, superstability, and period doubling, corresponding to the completely emaciated arm of the body. Similarly, the other arm ($\delta$) and both the legs ($\epsilon$ and $\zeta$) have reduced to zero thickness in the limit. Recall (see Fig. 3) that it is the emaciation of the arm which causes the transit of the lower part of where the arm and torso merge across the one-parameter path of Fig. 2, and which eventually renders invisible the creation by tangent bifurcation of corresponding orbit, so that the orbit becomes visible only when the torso is entered. The torso's boundaries in the limit are degenerate period-doubling and superstable curves ($\beta$ and $\gamma$). The orbits whose bodies are depicted in Fig. 14 are members of the main Farey sequences. The torsos of the orbits belonging to these sequences occupy the wedge between $b=0$ and the overlap boundary with full measure in the infinite-$s$ limit.[19,20]

The Farey sequence orbits have DSO's with no iterates on the interval between the turning points. For orbits whose DSO's do have iterates on this interval, where the slope is increasing without limit as $s\to\infty$, the arcs of the one-stroke representation become needlelike, with the result that the region where the orbit is stable has vanishing area. Figure 16 shows the evolution of the body of such an orbit: a doubling of the $1^1$ [which was shown in Fig. 3(a)]. The period-doubling cascades of the principal bodies become ever less observable as $s$ increases, allowing for the growing predominance of their Farey intermediate states migrating from higher $b$. A similar fate exists

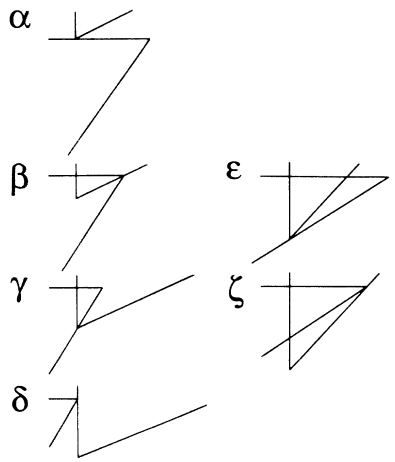


FIG. 15. Labeled points of Fig. 14(b) in the one-stroke representation. Upright (sideways) arc is $Z^3$ ($Z^2$). ($\alpha$) degenerate exterior tangent and period-doubling (arm); ($\beta$) degenerate period halving and superstable (entering torso); ($\gamma$) as ($\beta$) (leaving torso); ($\delta$) as ($\alpha$) (other arm); ($\epsilon$) degenerate internal tangent and period doubling (leg); ($\zeta$) as ($\epsilon$) (other leg).

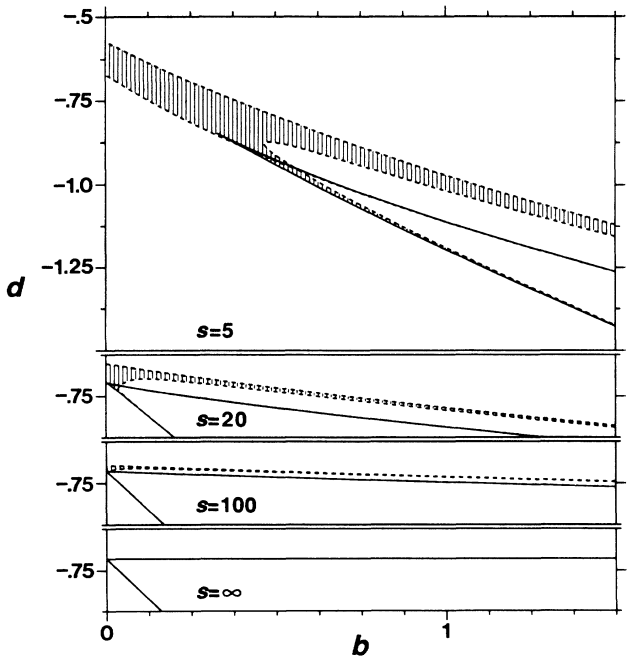


FIG. 16. A doubling of $1^1$: an example of a body whose area vanishes as $s \to \infty$.

for orbits with DSO's asymptotic to the overlap boundary or beyond (even those with no iterates on the interval between the turning points). The body of the $2^2$ orbit is shown in Fig. 17 as an example. As with the doubling of the $1^1$, the bi-SSO approaches the DSO leaving no torso in the limit, and all that remains of these bodies in the limit is their degenerate superstable skeleton.

The measure of chaos in the wedge between $b=0$ and the overlap boundary vanishes as $s$ tends to infinity. This can readily be understood by performing the transformation $x'=\ln[x-1/(1-a)]$. With this coordinate, positive contributions to a Liapunov exponent in the wedge can be obtained only in the interval between the turning points. The preimage sequence of this vanishing interval escapes entirely from the invariant interval except on a vanishing measure of the wedge.

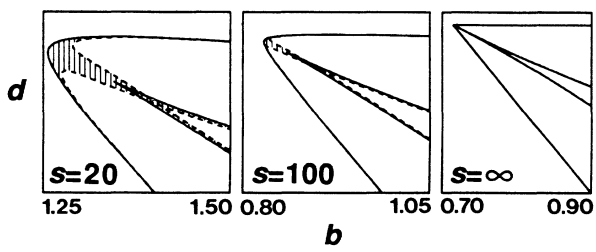


FIG. 17. $2^2$ another example of a body whose area vanishes as $s \to \infty$. The scales are the same in all pictures. The range in $d$ is 0.2.

## V. FAREY SEQUENCES CONTRASTED

In the preceding sections we have seen how a variety of experimentally observed one-parameter dynamical sequences can be placed on a continuous spectrum of behavior, and we have analyzed the diversity and continuity of this spectrum in some detail. In this way we have gained considerable knowledge about a mechanism for generating a Farey sequence that the evidence suggests is likely to be operating in physical systems. This mechanism has its own signatures which are different from those of motion on a torus, and in this section we summarize those differences as they are reflected (a) in one-parameter sequences and (b) in two-parameter surveys.

### A. One-parameter sequences of behavior

In a system that can be represented by a two-extremum map such as $Z$, the bodies of the Farey sequence states are distributed in the parameter plane on a Farey tree [see Figs. 3(b) and 10, and Ref. 43]. Consequently, a typical parameter path intersects a finite number of them. For example, the $1^1 1^1 1^2$ state does not appear on the parameter path of Fig. 2(d) [see Fig. 3(b)]. In contrast, along a parameter path in monotone circle maps, by which motion on a torus can be represented, the complete set of Farey intermediate states of the end points appears (limited only by observational resolution). Thus in an experimentally observed Farey sequence, the definite absence of some Farey intermediate states is a strong signature of a two-extremum map as the underlying mechanism.

Additionally in systems representable by the map $Z$, the boundaries of the Farey sequence states are period doublings rather than tangent bifurcations to quasi-periodicity. Exceptions, where the boundaries are tangent bifurcations—though to chaos not quasi-periodicity—are members of the sequence which are only marginally established on the parameter path; an example is the $1^4 1^5$ state in Fig. 2(b) [see Fig. 3(b)].

Evidently, when the comparison is between the behaviors represented by a slightly nonlinear shift map of the circle and by the map of the interval $Z$ at low $s$, there is little room for confusion. More difficult situations exist, however.

In experimental situations corresponding to high $s$ in $Z$, the character of the bifurcation boundaries may be hard to establish since the period-doubling cascades are highly compressed. Neither would the technique of using perturbations on the stable side of the boundary to characterize eigenvalues be effective due to the proximity of the superstable curve to the bifurcation boundary (see Fig. 15).

Furthermore, the incompleteness—note that we mean incomplete in membership, not just in measure—of the Farey sequence is harder to establish for situations corresponding to very large $s$ in $Z$; as $s$ approaches infinity the sequence on a path such as those of Fig. 2 becomes complete in the senses of both membership and measure. Note that in Fig. 3(c) we showed bodies of only a handful of the Farey sequence states; the complete set fills the entire measure of the wedge between $b=0$ and the overlap

boundary.[19,20] Measure-complete Farey sequences are also seen in marginally noninvertible, or "critical," circle maps,[46] as well as invertible circle maps with a near discontinuity.[36] However, differences exist. Universality results have been obtained for the scaling in critical circle maps.[46] In contrast, the scaling of large-$s$ Farey sequences in $Z$ is highly variable and nonuniversal. One can see from Fig. 3(c) that the predominance of the principal states $(1^1, 1^2, 1^3, \ldots)$ ranges from total, on $b=0$, to zero on the overlap boundary. (The tips of the Farey sequence torsos are dense on the overlap boundary.) In fact, while the dimension of the complementary set is zero on all paths to the low-$b$ side of the overlap boundary,[19] practical algorithms for its determination, such as those of Refs. 8, 46, and 47, yield a completely variable answer from zero on $b=0$ to 1 on the overlap boundary, rather than the universal value 0.87... for critical circle maps. In any case, values much different from 0.87 should suggest that a high-$s$ two-extremum map be considered as a possible mechanism.

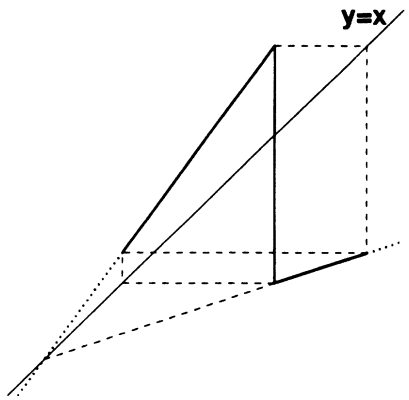


FIG. 18. The map $Z$ on the overlap boundary in the infinite-$s$ limit. $a=1.4$, $c=1$, $b=0.338\,734$, $d=-1.653\,163$, $-2.9 \le x \le 1.4$. On the boundary in the limit, the common point of intersection with the $y=x$ line of the parts of the map with slope $a$ and slope $b$ leads to the phenomenon of zero Liapunov exponent for almost all $x$.

### B. Two-parameter surveys

If experimental circumstances permit a two-parameter investigation, more opportunities naturally exist for ascertaining the mechanism of an observed Farey sequence. It is possible that an experimental parameter exist that is analogous to $s$ in $Z$.

The characteristic spectrum of behavior described in Sec. II would then be observable. However, there is reason to think that $(b,d)$ planes of $Z$ are more typical parameter planes than ones parallel to the $s$ axis, and in the following we allow for the most difficult case that the effective $s$ value remains fixed in a two-parameter experiment.

The two-parameter distribution of the bodies of the Farey sequence states in a situation representable by $Z$ at moderate $s$ [see Figs. 3(b) and 10, and Ref. 43] is radically different from the essentially one-dimensional arrangement of the Arnold tongues[48] of phase locking. In fact, the phase diagram for the two-extremum map has an extremely rich structure, with universal vector scaling,[13,49] and a universal asymptotic geometry[50] of the bodies of sequences of orbits such as the Farey subsequence $1^1, 2^1, 3^1, \ldots$.

However, if the choice is between a high-$s$ $Z$ mechanism and a torus mechanism, the possibility for confusion still exists because of the existence of a "pseudoquasiperiodic" line in $Z$ at infinite $s$: on the overlap boundary in the infinite-$s$ limit, almost every $x$ has zero Liapunov exponent. The behavior of $Z$ on this boundary thus resembles that of the shift map of the circle. Indeed, in the limit, $Z$ on the overlap boundary mimics a continuous piecewise linear map of the circle, as is illustrated in Fig. 18. Furthermore, the torsos of the Farey sequence bodies extending away toward $b=0$ resemble Arnold tongues in the respects of their denseness on the boundary and their increasing width away from it. Yet the two mechanisms for generating this quasiperiodic line can be distinguished by the neighboring phenomenology. In circle maps the line where quasiperiodicity has full measure is a boundary (or symmetry line) of the space of such maps. In $Z$ the line may be crossed into the region to the right where complex chaotic behavior predominates.

## VI. CONCLUSIONS

We have presented and analyzed in detail a model which accomplishes a unification of previously unrelated classes of dynamical behavior. This unification is important as it demonstrates that a wide variety of experimental observations can be generated by the same fundamental mechanism.

Moreover, we have shown how a U sequence and a Farey sequence can be transmuted one into the other by a smooth deformation that involves no change in the topology of the underlying mechanism. Thus is demonstrated the existence and characteristics of Farey sequences that arise in a manner quite different from that traditionally attributed to them. This kind of Farey sequence *cannot* occur on an invariant torus; the main periodic windows are separated by bands (possibly very narrow) of period doublings and chaos.

We have supported the significance of our model to experimental observations by referring to similar one-dimensional maps derived from data, and by demonstrating a correspondence between the spectrum of behavior generated by the model and results in the experimental literature. Given the result that there is more than one kind of Farey sequence that may be observed in experiments, we have, in order to facilitate their correct identification, discussed the differences between the respective phenomenologies, as well as their potentially confusing similarities.

A family of maps related to ours has been derived by Ding[51] from an impulsively forced oscillator model, thus

identifying a class of systems in which the phenomena analyzed here will be exhibited. We believe, however, that the contexts for maps of this kind are broader than this,[9] and therefore that further important work on how such maps arise remains to be done.


## ACKNOWLEDGMENTS

Acknowledgment is made to the Donors of the Petroleum Research Fund, administered by the American Chemical Society, for the support of this research.


---

*Present address: Center for Fluid Mechanics, Brown University, Providence RI 02912.


[1]R. Simoyi, A. Wolf, and H. L. Swinney, Phys. Rev. Lett. **49**, 245 (1982).

[2]J. Testa, J. Perez, and C. Jeffries, Phys. Rev. Lett. **48**, 714 (1982).

[3]M. Bier and T. C. Bountis, Phys. Lett. **104A**, 239 (1984).

[4]E. Knobloch and N. O. Weiss, Physica **9D**, 379 (1983).

[5]U. Parlitz and W. Lauterborn, in *Proceedings of the 12th International Congress on Acoustics,* edited by T. Embleton *et al.* (Beauregard, Toronto, 1986), p. I4-7.

[6]K. Coffman, W. D. McCormick, H. L. Swinney, and J. C. Roux, in *Nonequilibrium Dynamics in Chemical Systems,* edited by C. Vidal and A. Pacault (Springer, New York, 1984).

[7]J. M. T. Thompson and H. B. Stewart, *Nonlinear Dynamics and Chaos* (Wiley, New York, 1986), Chap. 15.

[8]J. Maselko and H. L. Swinney, J. Chem. Phys. **85**, 6430 (1986).

[9]F. N. Albahadily, J. Ringland, and M. Schell, J. Chem. Phys. **90**, 813 (1989).

[10]W. Lauterborn and I. Eick, J. Opt. Soc. Am. B **5**, 1089 (1988).

[11]G. Hardy and E. Wright, *An Introduction to the Theory of Numbers* (Clarendon, Oxford, 1979).

[12]S. Fraser and R. Kapral, Phys. Rev. A **25**, 3223 (1982).

[13]S. Fraser and R. Kapral, Phys. Rev. A **30**, 1017 (1984).

[14]S.-J. Chang, M. Wortis, and J. Wright, Phys. Rev. A **24**, 2669 (1981).

[15]R. Perez and L. Glass, Phys. Lett. **90A**, 441 (1982).

[16]L. Glass and R. Perez, Phys. Rev. Lett. **48**, 1772 (1982).

[17]L. Glass, M. Guevara, J. Bélair, and A. Shrier, Phys. Rev. A **29**, 1348 (1984).

[18]J. Bélair and L. Glass, Physica **16D**, 143 (1985).

[19]J. Nagumo and S. Sato, Kybernetik **10**, 155 (1972); S. Yoshizawa, H. Osada, and J. Nagumo, Biol. Cybernetics **45**, 23 (1982).

[20]E. J. Ding and P. C. Hemmer, J. Stat. Phys. **46**, 99 (1987).

[21]P. Mandel and R. Kapral, Opt. Commun. **47**, 151 (1983).

[22]P. Nardone, P. Mandel, and R. Kapral, Phys. Rev. A **33**, 2465 (1986).

[23]P. Gaspard, R. Kapral, and G. Nicolis, J. Stat. Phys. **35**, 697 (1983).

[24]A. Arneodo, P. Coullet, E. Spiegel, and C. Tresser, Physica **14D**, 327 (1985).

[25]E. Celarier and R. Kapral, J. Chem. Phys. **86**, 3357 (1987).

[26]D. M. Lindberg, Ph.D. thesis, University of Texas, 1988.

[27]M. Rabinovich and A. Fabrikant, Zh. Eksp. Teor. Fiz. **77**, 617 (1979) [Sov. Phys.—JETP **50**, 311 (1979)].

[28]K. Coffman, W. D. McCormick, Z. Nosticzius, R. Simoyi, and H. L. Swinney, J. Chem. Phys. **86**, 119 (1987); see also P. Richetti, J. C. Roux, F. Argoul, and A. Arneodo, *ibid.* **86**, 3339 (1987); A. S. Pikovsky, Phys. Lett. **85A**, 13 (1981).

[29]O. Decroly and A. Goldbeter, J. Theor. Biol. **124**, 219 (1987).

[30]T. H. Yoon, J. W. Song, S. Y. Shin, and J. W. Ra, Phys. Rev. A **30**, 3347 (1984); J. W. Song, T. H. Yoon, and S. Y. Shin, J. Opt. Soc. Am. B **1**, 488 (1984); S. Tanka, T. Matsumoto, and L. O. Chua, Physica **28D**, 317 (1987).

[31]L. Q. Pei, F. Guo, S. X. Wu, and L. O. Chua, IEEE Trans. Circuits Syst. **CAS-33**, 438 (1986).

[32]R. Van Buskirk and C. Jeffries, Phys. Rev. A **31**, 3332 (1985).

[33]P. Collet and J. P. Eckman, *Iterated Maps of the Interval as Dynamical Systems* (Birkhauser, Boston, 1980).

[34]N. Metropolis, M. Stein, and P. Stein, J. Comb. Theory **15**, 25 (1973).

[35]R. Bagley, G. Mayer-Kress, and J. Farmer, Phys. Lett. A **114**, 419 (1986); J. Maselko and H. L. Swinney, *ibid.* **119**, 403 (1987); M. Schell and F. N. Albahadily, J. Chem. Phys. **90**, 822 (1989); J. L. Hudson and J. C. Mankin, J. Chem. Phys. **74**, 6171 (1981).

[36]D. Barkley, Phys. Lett. A **129**, 219 (1988).

[37]Z. Noszticzius, W. D. McCormick, and H. L. Swinney, J. Phys. Chem. **93**, 2796 (1989).

[38]This pair of curves has been termed the "skeleton" of the orbit (see Ref. 16).

[39]C. Genis, J. Math. Biol. **24**, 291 (1986); R. P. Pascual and J. Lomnitz-Adler, Physica D **30**, 61 (1988).

[40]K. Kaneko, Prog. Theor. Phys. **72**, 1089 (1984).

[41]R. S. Mackay and C. Tresser, Physica **27D**, 412 (1987).

[42]J. Ringland and M. Schell (unpublished).

[43]J. Ringland and M. Schell, Phys. Lett. A **136**, 379 (1989).

[44]No numerical counterexamples have been observed.

[45]J. Milnor and W. Thurston, in *Dynamical Systems,* Vol. 1342 of *Lecture Notes in Mathematics,* edited by A. Dold and B. Eckman (Springer, New York, 1988), p. 465.

[46]P. Cvitanovic, M. Jensen, L. Kadanoff, and I. Procaccia, Phys. Rev. Lett. **55**, 434 (1985).

[47]H. L. Swinney and J. Maselko, Phys. Rev. Lett. **55**, 2366 (1985).

[48]V. I. Arnold, *Geometrical Methods in the Theory of Ordinary Differential Equations* (Springer, New York, 1983), pp. 95–109.

[49]M. Schell, S. Fraser, and R. Kapral, Phys. Rev. A **28**, 373 (1983).

[50]J. Ringland and M. Schell (unpublished).

[51]E. Ding, Phys. Rev. A **34**, 3547 (1986); **35**, 2669 (1987).